ISSN No: 2348-4845
International Journal & Magazine of Engineering, Technology, Management and Research
A Peer Reviewed Open Access International Journal

High Power Approach of Solar Clump Simulater to Provide PV System Testing By Using LLC Resonant Converter

B.Swathi
M.Tech-PE,
Vidya Bharathi Institute of Technology, T.S, India.

L.Ramesh
Associate Professor,
Vidya Bharathi Institute of Technology, T.S, India.

Abstract:
In this paper, a high-efficiency solar array simulator (SAS) implemented by an LLC resonant dc–dc converter is proposed to save the cost and energy of photovoltaic (PV) system testing. The proposed converter has zero-voltage switching (ZVS) operation of the primary switches and zero-current switching (ZCS) operation of the rectifier diodes. By frequency modulation control, the output impedance of an LLC resonant converter can be regulated from zero to infinite without shunt or serial resistors. Therefore, the efficiency of the proposed SAS can be significantly increased. The circuit operations are analyzed in detail to derive the theoretical equations. Circuit parameters are designed based on the practical considerations. Finally, an illustrative example is implemented to demonstrate the feasibility of the proposed SAS.

Index Terms:
LLC resonant dc–dc converter, photovoltaic (PV) system, solar array simulator (SAS)

INTRODUCTION:

Recently, residue of traditional energy resources (i.e., fossil energy) is highly limited and would be exhausted in the near future. Besides, combustion of fossil fuels results in a serious threat of global warming. Hence, developing renewable energy resources to replace traditional ones has been a research of great urgency. Among all renewable energy resources, photovoltaic (PV) energy becomes most attractive recently, because it is noiseless, pollution-free, nonradioactive, and inexhaustible. Since the output PV characteristics are influenced by illumination and temperature, the maximum power Point tracking (MPPT) is a necessary technology in PV applications. Atmospheric conditions are uncontrollable so that PV system engineers cannot obtain the corresponding PV characteristics to qualify the feasibility and dynamic response of their MPPT approaches immediately. In order to relieve this difficulty, metal-halide lamps and temperature controlling devices are used to control the illumination and temperature of PV arrays. But the temperature controlling devices are very expensive, and the power consumption of driving metal-halide lamps results in additional energy waste. Therefore, the literatures propose several solar array simulators (SASs) which can provide PV characteristics directly. Among them, the most applicable approach in high-power systems is using pulse width modulation (PWM) dc–dc converters to generate PV characteristics.

However, shunt resistors are required to limit output voltage at extremely high duty-ratio, and serial resistors are used to inhibit spike current at extremely low duty-ratio operation. These resistors cause additional power dissipations and lower conversion efficiency. Furthermore, the power switches of PWM converters operate in hard switching, which will result in high switching losses and electromagnetic interference (EMI) issues. Theoretically, the output impedance of resonant converters can be regulated from zero to infinite by applying frequency modulation control. Because it can match that of PV output characteristics without shunt or serial resistors, resonant converters are more applicable than the traditional PWM dc–dc converters for the SAS applications.

ISSN No: 2348-4845
International Journal & Magazine of Engineering, Technology, Management and Research
A Peer Reviewed Open Access International Journal

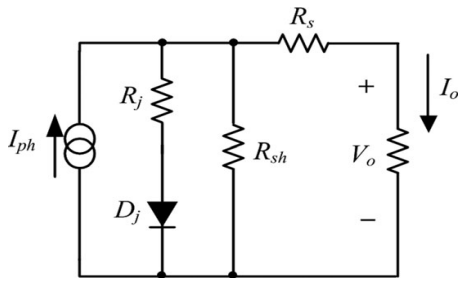

Figure 1: Equivalent circuit of a solar cell

PV System Modeling:

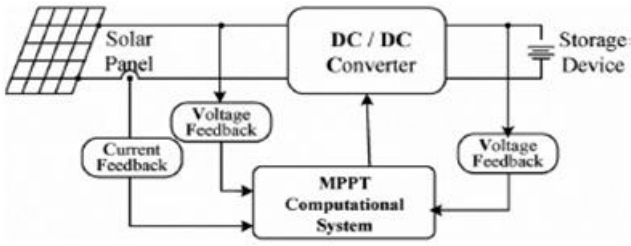

Figure 2: Block Schematic of the System

Maximum Power Point Tracker:

The main idea is based on the graphical interpretation of the maximum power point as the intersecting point of two curves on the phase plane corresponding to the solution of two algebraic equations. In other words, the operating point is the intersecting point of the PV-array characteristic curve and the maximum power line. Due to the high initial installation cost and the low energy conversion efficiency, a maximum power point tracking (MPPT) control for the solar array is essential in a photovoltaic power system.

Equivalent Circuit for the Solar Panel:

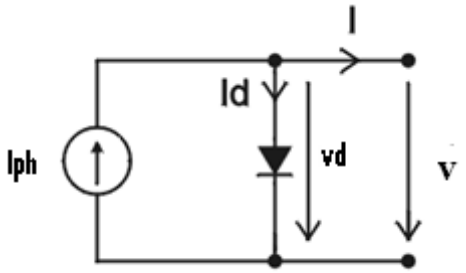

Figure 3: Equivalent Circuit of Solar Panel

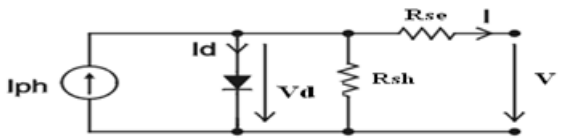

Figure 4: Real Solar Cell Model with Series and Parallel Resistances

A solar cell module is the basic element of each photovoltaic system. It consists of many jointly connected solar cells. A number of solar cell models have been developed, but the one diode electrical equivalent circuit is commonly used for cell based or module based analysis. It consists of a diode, a current source, a series resistance and a parallel resistance. The current source generates the photo-current that is a function of the incident solar cell radiation and temperature.

DC-DC CONVERTER TOPOLOGIE:

In power systems, based on battery sources and super capacitors have been increased. Unfortunately, the output voltages of these sources are relatively low. Therefore the step-up power conversion is required in these systems. Besides the step-up function, the demands such as low current ripple, high efficiency, fast dynamics, light weight, and high power density have also increased for various applications. Input current ripple is an important factor in a high step-up dc/dc converter. Especially in the fuel cell systems, reducing the input current ripple is very important because the large current ripple shortens fuel cell's lifetime as well as decreases performances. Therefore, current-fed converters are commonly used due to their ability to reduce the current ripple.

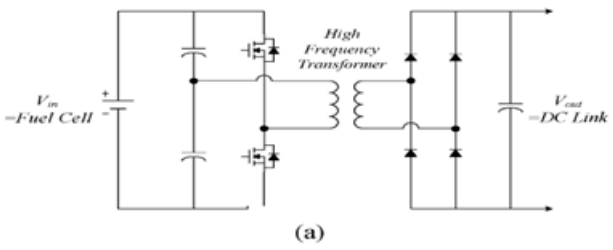

Figure 2 voltage- fed dc–dc converter.

ISSN No: 2348-4845
International Journal & Magazine of Engineering, Technology, Management and Research
A Peer Reviewed Open Access International Journal

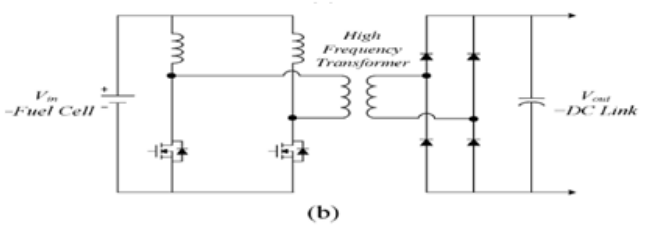

Figure 6: current-fed dc-dc converter

LLC RESONANT DC–DC CONVERTER:

The circuit diagram of an LLC resonant dc–dc converter is shown in Fig. 2, which consists of an LLC resonant inverter, a current-driven transformer with a center-tapped rectifier. The topology of LLC converter is very similar to that of SRC. The main difference is that the magnetizing inductance $L_m$is only slightly higher than the resonant inductance $L_r$in the LLC converter. Therefore, at some load conditions, Lm may participate in the resonance with $L_r$and $C_r$and change the characteristics of resonant tank.

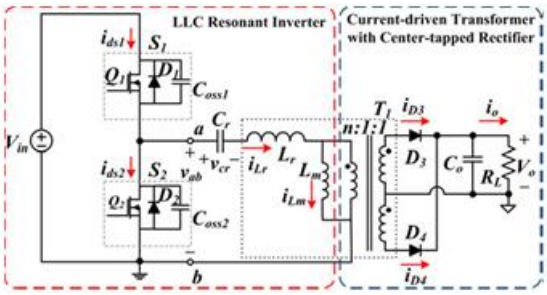

Figure 7: Circuit diagram of LLC resonant dc/dc converter.

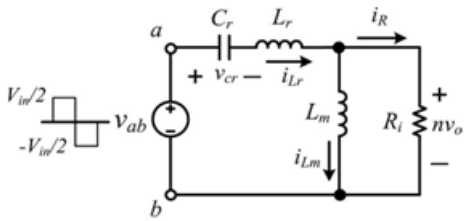

Figure 8: Equivalent circuit of the LLC resonant converter.

The equivalent circuit of the LLC resonant inverter can be depicted as shown in Fig.8, in which $R_i$is equivalent load resistance seen in primary side, and can be expressed as R_i= 8n2RL /π2 .

The input symmetrical square waveform v_{ab} with the magnitude of V_{in}/2 can be obtained by alternate conducting of power switches S_1 and S_2.

OPERATION PRINCIPLE OF THE LLC RESONANT

DC–DC Converter

As shown in Fig. 7, the primary switches S_1 (S_2) are composed of an MOSFET Q_1 (Q_2), and its intrinsic anti parallel diode D1 (D2) and equivalent output capacitor C_{OSS1} (C_{OSS2}). The resonant tank is formed by the resonant capacitor C_r, and the leakage inductor $L_r$and magnetizing inductor $L_m$of the transformer T_1. By conducting the switches S_1 and S_2 alternately, a symmetrical square waveform with the magnitude of V_{in} /2 can be obtained in the input terminal of the resonant tank, where V_{in} is the input voltage. The center-tapped rectifier is constructed by connecting diodes D_3 and D_4 to the secondary windings of T_1.Based on the analysis of earlier section, the main theoretical

Mode 1:

This mode starts when the switch S_1 is turned ON under ZVS. The equivalent circuit is shown in Fig. 9(a). The resonant current $i_{Lr}$is sine-wave and increases from negative to discharge C_r, and energy returns to the input voltage source. The voltage of $L_m$is clamped to nV_Oso that the magnetizing current i_{Lm} increases linearly from negative. The energy stored in Lm will be released through D_3 to output load. When i_{Lr}reaches zero, this mode ends.

Mode 2:

As shown in Fig. 9(b), since i_{Lr}increases from zero to positive, the input voltage source charges $C_r$and L_r, and supplies energy to output load simultaneously. The energy in $L_m$is released to output load continuously. When i_{Lm}reaches zero, this mode ends.

Mode 3:

At this mode, because the voltage of Lm is still clamped to nV_O, i_{Lm}remains increasing linearly.

ISSN No: 2348-4845
International Journal & Magazine of Engineering, Technology, Management and Research
A Peer Reviewed Open Access International Journal

The input voltage source charges Lm and supplies energy to output load. The equivalent circuit is shown in Fig 9(c).

Mode 4:

This mode starts when $i_{Lr}$and i_{Lm}equal each other. Current circulating through the secondary diode D_3 naturally decreases to zero so that this diode turns OFF under ZCS condition. The voltage spike caused by diode reverse recovery would not exist. The voltage of Lm is no longer clamped to nV_O, hence, Lm is in series with Lrand participates in the resonance with Cr. The equivalent circuit of this mode is shown in Fig. 9(d). Because the equivalent inductance of (Lr+ Lm) is higher than Lr, as shown in Fig. 8, $i_{Lr}$and $i_{Lm}$are almost constant in this short time interval.

Mode 5:

As shown in Fig 9(e). while S_1 is turning OFF, the resonant current $i_{Lr}$is charging C_{OSS1} and discharging C_{OSS2} simultaneously. At the moment of vds2 decreasing to zero, the resonant current i_{Lr} flows through anti paralleled diode D_2 which provide ZVS operation for S_2 turn ON. At the same time, the secondary rectifier diode D_4 turns ON. The voltage of Lm is clamped to nV_O with reverse polarity so that the current i_{Lm} becomes decreasing linearly. The magnetizing inductor Lm is separated from the resonance with Cr .When S_2 turns ON under ZVS, this mode ends and enters the half cycle with symmetrical operation principles.

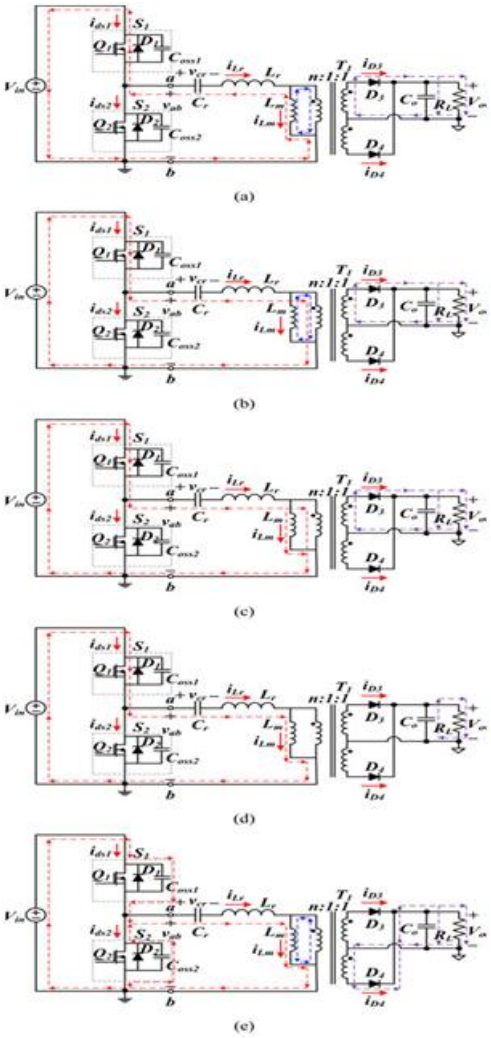

Figure 9 Equivalent circuits of (a) Mode 1, (b) Mode 2, (c) Mode 3, (d) Mode4, and (e) Mode 5 for the LLC converter operating in region 2.

MATLAB MODEL DIAGRAMS:

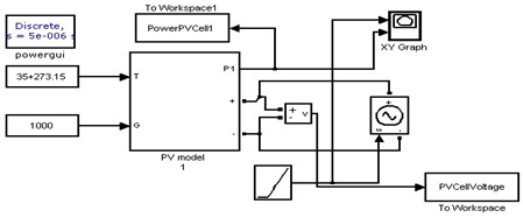

Figure 10: PV SYSTEM

ISSN No: 2348-4845
International Journal & Magazine of Engineering, Technology, Management and Research
A Peer Reviewed Open Access International Journal

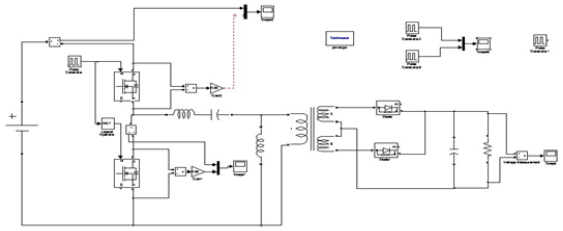

Figure 11: WITH OUT LLC RESONANT DC-DC CONVERTER

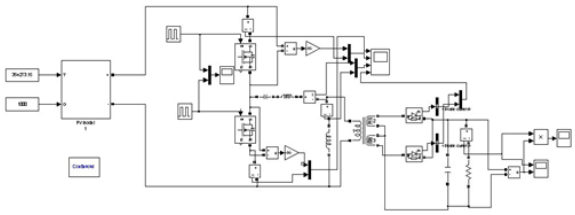

Figure 12: WITH LLC RESONANT DC-DC CONVERTER

RESULTS:

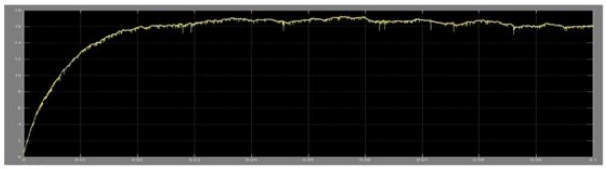

Figure 13:3 WAVE FORM WITH OUT LLC DC-DC CONVERTER

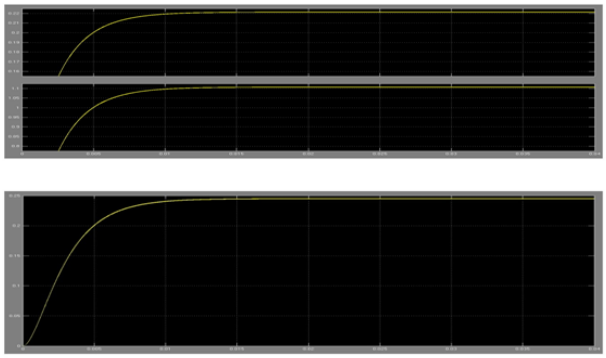

Figure 14:4 WAVE FORM FOR LLC RESONANT DC-DC CONVERTER

CONCLUSION:

A reliable and simple scheme integrating wind-driven induction generators and PV array has been successfully developed for the first time to supply a three-phase remote load with constant frequency balanced voltages. The generation system will supply constant voltages with varying wind speed and irradiation when the battery is switched on. The hybrid system is cost-effective and requires a simple interface for integration, thus making it suitable for off-grid applications. The independent control of real and reactive power supplied to the load is achieved with the help of SRF theory along with the load balancing, load compensation and harmonic distortion compensation. A dc–dc step-up converter can be interposed in the proposed system between the PV array and the inverter to maintain the PV array voltage constant for varying atmospheric conditions. The same converter can track the peak-power point of the PV array when the battery is switched to the system.

REFERENCES:

[1] D. G. Infield, G. W. Slack, N. H. Lipman, and P. J. Musgrove, “Review of wind/diesel strategies,” Proc. Inst. Elec. Eng. A, vol. 130, no. 9, pp.613–619, 1983.

[2] A. J. Tsitsovits and L. L. Freris, “Dynamics of an isolated power system supplied from diesel and wind,” Proc. Inst. Elec. Eng. A, vol. 130, no 9, pp. 587–595, 1983.

[3] O. Honorati, G. L. Bianco, F. Mezzetti, and L. Solero, “Power electronic interface for combined wind/PV isolated generating system,” in Proc. European Union Wind Energy Conf., Goteborg, Sweden, 1996, pp. 321–324.

[4] S. A. Daniel, K. Pandiaraj, and N. Jenkins, “Control of an integrated wind-turbine generator and photovoltaic system for battery charging,” in Proc. 19th British Wind Energy Conf., Edinburgh, U.K., 1997, pp. 121–128.

ISSN No: 2348-4845
International Journal & Magazine of Engineering, Technology, Management and Research
A Peer Reviewed Open Access International Journal

[5] B. S. Borowy and Z. M. Salameh, "Dynamic response of a stand-alone wind energy conversion system with battery energy storage to a wind gust," IEEE Trans. Energy Conversion, vol. 12, pp. 73–78, Mar. 1997.

[6] California Energy Commission, "2008 energy policy report update," 2008.

[7] R. Spee and J. H. Enslin, "Novel control strategies for variable-speed doubly fed wind power generation systems," Renewable Energy, vol. 6, pp. 907–915, 1995.

[8] P. Novak, T. Ekelund, Y. Jovik, and B. Schmidtbauer, "Modeling and control of variable-speed wind-turbine drive system dynamics," IEEE Control Syst. Mag., vol. 15, no. 4, pp. 28–37, Aug. 1995.

[9] T. Thiringer and J. Linders, "Control by variable rotor speed of fixed-pitch wind turbine operating in speed range," IEEE Trans. Energy Conv., vol. 8, no. 3, pp. 520–526, Sep. 1993.

[10] M. G. Simoes, B. K. Bose, and R. J. Spiegel, "Fuzzy logic based intelligent control of a variable speed cage machine wind generation system," IEEE Trans. Power Electron., vol. 12, no. 1, pp. 87–95, Jan. 1997.